THESIS

Collective Escape Behaviour in Springtails:
Effects of Population Density on Movement Synchrony
and Escape Response Dynamics

by Zhannur Nurlan
MSc General Biology

Supervisors: Oláh Gergő, Prof. Dr. Zoltán Barta
University of Debrecen, Faculty of Science and Technology
Department of Evolutionary Zoology and Human Biology

Debrecen, 2026

Introduction

Collective movement, where individuals act without any central guidance, is one of the most intriguing and scientifically compelling phenomena in biology. From flocks of birds to vast marching bands of locust nymphs sweeping across the African savanna, coordinated group motion emerges across nearly every major animal taxon, spanning orders of magnitude in both organism size and group scale (Vicsek and Zafeiris, 2012). Despite this variety, the underlying principle is remarkably consistent: coordinated group behaviour emerges not from any single directing individual, but from repeated local interactions between neighbouring animals following simple behavioural rules (Couzin et al., 2002; Vicsek and Zafeiris, 2012). This formation of global order from local interactions has made collective animal motion one of the central topics in modern behavioural ecology.

The variables that govern whether and how collective motion emerges are well established theoretically. Population density is among the most important: below a critical density, individuals interact too infrequently for coordination to propagate through the group, and motion remains disordered; above it, alignment spreads rapidly and ordered collective movement emerges (Vicsek and Zafeiris, 2012). This transition between disordered and ordered states has been formally characterised as a phase transition. Empirical confirmation of this transition was best demonstrated in locust nymphs marching in circular laboratory arenas, where the proportion of time spent in an ordered collective state increased sharply with group size, and directional switching between clockwise and counterclockwise motion became increasingly rare as density rose (Ariel and Ayali, 2015). These findings established that the theoretical predictions of self-propelled particle models translate to real biological systems, and that density is not merely a quantitative parameter, but a driver of qualitative change in collective behaviour.

Recent technological advances in individual motion tracking have significantly transformed the study of collective motion over the last few decades. For much of the field's history, data collection was limited to observational snapshots, and quantitative analysis of individual trajectories within large groups was technically impossible, leaving theoretical modelling as the primary tool for understanding collective dynamics (Vicsek and Zafeiris, 2012). However, the development of high-resolution GPS logging, drone-based aerial videography, high-speed cameras, and computer vision tracking software has since made it possible to reconstruct the complete movement trajectories of every individual in a group simultaneously and in fine spatiotemporal detail. For instance, Nagy et al. (2010) equipped flocks of up to ten homing pigeons with lightweight GPS loggers recording at 0.2-second

intervals and used directional cross-correlation analysis to reveal a well-defined and consistent hierarchical leader-follower network; a result that would have been entirely impossible without collected individual-level high-resolution data. More recently, Ozogány et al. (2023) demonstrated that as little as five minutes of drone-based movement tracking of a herd of 238 Przewalski's horses was sufficient to reconstruct the herd's multilevel social structure, identify various kinship-based association patterns, and even predict future group membership changes, suggesting that short, intensive movement recordings can potentially substitute or complement years of behavioural observation. Beyond the practical advances, theoretical modelling has also remained essential for generating testable predictions about how variables such as density, social network structure, and interaction range shape the group's dynamics (Bode et al., 2010; Bode et al., 2011).

Despite the extensive progress in understanding collective motion among vertebrates and a small group of invertebrates, such as locusts, the vast majority of terrestrial arthropods still remain critically understudied. This poses a significant gap, given that the group represents a numerically and ecologically important component of terrestrial animal communities. Particularly, the coordinated reaction of a population to an acute disturbance stimulus, also known as the collective escape response (Domenici et al., 2011), has received far less attention in comparison to sustained directed movement such as marching or flocking. It remains unclear whether disturbance responses in dense invertebrate populations propagate collectively through local interaction or whether individuals respond independently to the same shared stimulus. Furthermore, while density is theoretically predicted to drive transitions between individual and collective response modes (Vicsek and Zafeiris, 2012; Ariel and Ayali, 2015), this prediction has rarely been tested under fully controlled laboratory conditions for short-duration escape responses in small arthropods.

Springtails (*Folsomia candida*) represent an exceptionally convenient model organism for studying these gaps. These animals can populate up to 100,000 individuals per square metre of soil in certain habitats (Hopkin, 1997) and are known to be ecologically significant decomposers and key participants of soil nutrient cycling. Their primary escape mechanism is the furcula: a forked appendage held under tension beneath the abdomen by a latch structure, released explosively upon mechanical disturbance to launch the animal distances of up to 100 times its body length (Sudo et al., 2015). From a methodological standpoint, springtails offer several advantages that are difficult to achieve with vertebrate study systems: their reproductive rate is high, allowing population density to be easily controlled; their growth requirements are simple and financially accessible; and, being confined to an enclosed petri dish, no individual can leave the field of view during recording. Most importantly, the presumed absence of

individual recognition in F. candida means that their interaction network constitutes a pure communication network based on mechanosensory proximity, free from social preferences that complicate the interpretation of interaction data that is seen in vertebrates such as equines (Bode et al., 2010; Ozogány et al., 2023). This simplicity makes springtails conceptually cleaner test subjects for examining the fundamental relationship between density, interaction rate, and collective dynamics.

This paper investigates collective escape behaviour in springtail populations under two density conditions (high and low) using high-quality slow-motion video recording and individual movement tracking to characterise both individual-level and population-level responses to a standardized mechanical disturbance. Drawing direct inspiration from Ozogány et al. (2023), who demonstrated that short recordings of fine-scale movement combined with high-throughput data-driven analysis can reveal intriguing population-level dynamics inaccessible to traditional observational methods, we apply an analogous approach at a smaller scale: using seconds of camera footage rather than minutes of drone video, and individual springtails rather than horses, to study and analyze the dynamics of collective movement.

This study hypothesizes that high-density populations will show greater between-individual movement synchrony, faster propagation of the escape response through the population, and more spatially aggregated distributions than low-density populations, consistent with theoretical predictions that increasing density drives transitions toward collective ordered motion through more frequent and more connected local interactions (Vicsek and Zafeiris, 2012; Ariel and Ayali, 2015). It tests density-dependent collective dynamics in a short-duration escape context rather than sustained directed movement, addressing an understudied aspect of collective behaviour with direct ecological relevance. Finally, the manually annotated trajectory dataset produced constitutes a foundation for future machine learning automation of springtail tracking, with the potential to make this approach scalable to larger experimental designs and other small arthropod systems.

Materials and Methods

Springtail colonies were grown on standard petri dishes (90mm diameter), on a base of plaster of paris mixed with charcoal, fed dried yeast (Saccharomyces cerevisiae), and kept at a constant temperature in dim light. Animals used in experiments were drawn from stock cultures of mixed age, with juveniles and adults present, reflecting the natural age structure of a growing population.

Experimental design

A total of six petri dish arenas were prepared, divided into two density treatment groups: three high-density populations (between 350 and 470 individuals) and three low-density populations (between 70 and 150 individuals). Each petri dish constituted a single biological replicate. These density levels were selected to bracket the range of densities likely to produce qualitatively different collective dynamics (Vicsek and Zafeiris, 2012; Ariel and Ayali, 2015). The exact individual counts, determined by manual tracking annotation, were: high-density plates P2T3 (n = 401), P3T3 (n = 356), and P5T3 (n = 470); low-density plates P1T3 (n = 140), P6T3 (n = 149), and P13T3 (n = 76) (Figure 1). Each dish was recorded on three separate occasions (Trial 1, Trial 2 and Trial 3), yielding eighteen recordings in total. However, data from Trial 1 and 2 were excluded from the final analysis due to limited time and tracking inconsistencies arising from technical difficulties during annotation, which produced high variation in tracked individual counts between trials that precluded valid cross-trial comparisons. Therefore, all analysis was made on six plates originating from the T3 recording session.

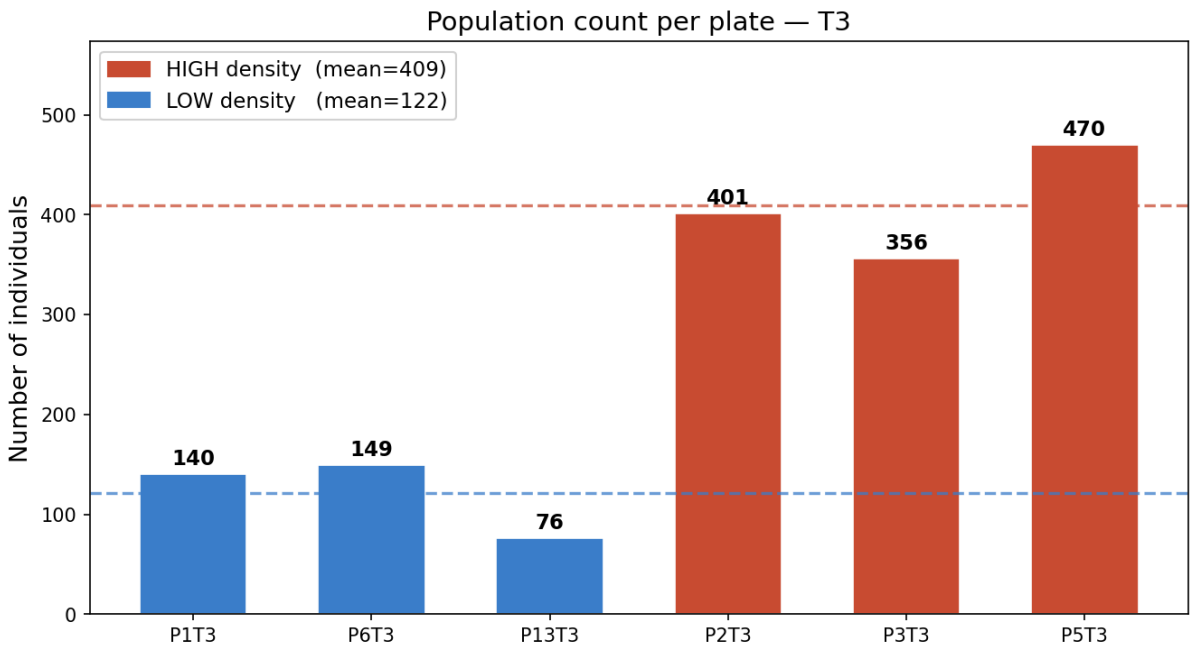

Figure 1. *Population count per plate. Bars indicate the total number of individually tracked springtails. Blue = low-density plates (P1T3, P6T3, P13T3); orange = high-density plates (P2T3, P3T3, P5T3). Dashed horizontal lines mark the respective group means (low: 122; high: 409).*

The escape response was a standardised mechanical disturbance: the rapid removal of the petri dish lid. This stimulus was chosen because it produces a consistent, reproducible vibration, which triggers the furcula-based escape jump in springtails. Lid removal was consistently performed by a single person to minimise variation in stimulus intensity. The time between the recordings was also standardised to allow enough time for the animals to calm down. All recordings began at the moment of lid removal and captured the immediate escape response and subsequent behavioural recovery within a fixed four-second window.

Each four-second recording produced 960 individual frames at 240 fps, of which 240 were selected for analysis, starting from lid opening and capturing only the moments where springtails were active, with the ends of recordings trimmed where movement ceased. Recordings were initiated immediately upon lid removal, with the first frame corresponding to the moment of disturbance. All trials were conducted in a quiet, vibration-isolated environment to prevent unintended disturbance stimuli during recording.

Equipment selection and optimisation

Before data collection, a systematic evaluation of recording equipment and conditions was conducted to identify the optimal setup for capturing individual springtail movement. Initial trials using a professional digital camera at standard frame rates (25–30 frames per second) were insufficient to resolve individual jump trajectories without motion blur, as the

furcula-driven escape jump is completed in a fraction of a second. Slow-motion recordings with the same professional digital camera also resulted in insufficient quality, as the recording quality significantly decreased with increased fps. The final recording setup used an Apple iPhone 13 smartphone camera operating in slow-motion mode at 240 frames per second (fps) and 4K resolution. The camera was placed 50cm above the petri dish and provided enough temporal resolution to capture the animal movement without motion blur.

Lighting conditions were optimised through iterative testing to maximise contrast between individual springtails and the petri dish substrate. Illumination angle and intensity were adjusted to eliminate reflective glare from the dish surface while ensuring that individual animals were clearly distinguishable across all frames.

Frame Extraction and Annotation

The extracted frames were analysed using the CVAT (Computer Vision Annotation Tool) software, an open-source annotation platform developed for computer vision and machine learning applications (Musleh et al., 2023). This platform allows a multi-object tracking workflow, has a frame-by-frame annotation interface, and is able to export tracking data in a structured coordinate format, thus making it perfectly suitable for this project.

Each individual springtail visible in the recording was manually annotated across the full sequence of 480 frames in 12 videos (of which 240 frames of 6 videos were used), producing a time series of x,y pixel coordinates for every individual throughout the two-second recording window. Coordinates were recorded at the centroid of each animal's body. Where animals were temporarily obscured by overlap with conspecifics or by the edge of the dish, interpolation between the last known and next observable position was used to maintain track continuity, following standard practice in manual trajectory annotation (Ozogány et al., 2023).

Data Processing and Coordinate Transformation

Annotation data was then exported from CVAT in XML format and parsed using a custom Python pipeline. Each annotated point was assigned a unique individual label and a frame index extracted directly from the source filename. Analysis was done only on the animals visible from the first frame. Pixel coordinates were converted to millimetres using the physical diameter of the petri dish (90mm) divided by its measured diameter in pixels (1017.5px), resulting in a conversion factor of ~0.09mm per pixel. All subsequent analyses were conducted in mm units.

Individual Movement Metrics

Instantaneous speed (mm/s) was calculated for each individual at each frame as the Euclidean distance between consecutive annotated positions divided by the inter-frame interval (1/240 s). The first frame of each individual's track was assigned NaN as no prior position was available.

Mean pairwise distance between all simultaneously tracked individuals was computed at each frame as the mean of all unique Euclidean distances between animal pairs, yielding a time series of group spread over the 240-frame observation window.

Spatial autocorrelation of speed was assessed at each frame using Moran's I statistic (Vicsek and Zafeiris, 2012). For each frame, a binary spatial weights matrix was constructed by thresholding pairwise inter-individual distances at 13.0 mm. Moran's I was then computed as:

$$I = (N / \Sigma W) \times (z'Wz / z'z)$$

where N is the number of individuals, W is the spatial weights matrix, and z is the vector of mean-subtracted instantaneous speeds. Values of Moran's I greater than zero indicate positive spatial autocorrelation, meaning spatially adjacent animals move at more similar speeds than expected by chance.

Collective Synchrony Analysis

To quantify collective synchrony in speed across the population, two complementary analytical approaches were applied to the full speed matrix (rows = frames, columns = individuals) for the first 240 frames of each recording.

Pairwise Speed Correlation. A pairwise Spearman correlation matrix was computed across all pairs of individuals using their 239-frame speed time series. The upper triangle of the resulting matrix provided the distribution of all pairwise Spearman r values (De Winter et al., 2016); the mean of this distribution was used as the primary summary metric of collective speed synchrony per plate.

Spatial–Behavioural Distance Correlation. To test whether spatial proximity predicted the degree of movement synchrony between pairs of individuals, a Spearman correlation was computed between pairwise spatial distance (Euclidean distance between mean positions across the recording) and pairwise behavioural distance (defined as 1 − Spearman r). A positive correlation indicates that spatially closer animals also showed more similar speed time series.

Spatial Grid Analysis

To characterise the spatial distribution and movement patterns within each arena, a 5×5 regular grid was overlaid on the 90×90 mm dish coordinate space, yielding 25 cells of 18×18 mm each. Cells whose geometric centre fell outside the circular dish boundary (radius = 45 mm, centred at (45, 45) mm) were excluded from all analyses and rendered as empty in spatial figures. All spatial analyses were performed on the first 240 frames only.

Mean grid occupancy was computed as the mean number of animals observed per cell per frame, averaged across all 240 frames. Spatial speed maps were computed as the mean instantaneous speed of all animals passing through each cell, averaged across all frames in which animals were present in that cell. Cells with zero total animal-frame observations across all 240 frames were assigned NaN and displayed as white grids in figures; this occurs in low-density plates where the animal count is insufficient to provide uniform arena coverage.

A 5×5 grid-based Spearman correlation was computed per frame between local animal density (count per cell) and local mean speed (mean instantaneous speed of all animals in that cell), providing a frame-by-frame measure of whether locally denser regions also moved faster.

Group centre of mass (CoM) was computed at each frame as the mean x and y coordinate in mm across all individuals present, and CoM displacement was calculated as the Euclidean distance from the initial CoM position at frame 0.

Group-Level Kinematics

Group polarisation $\Phi(t)$ was computed at each frame as the magnitude of the mean unit heading vector across all individuals. Individual headings were estimated from the direction of displacement between consecutive frames. A value of $\Phi = 1$ indicates perfect directional alignment; $\Phi = 0$ indicates uniformly random headings.

Radial and tangential velocity components were computed by decomposing each individual's velocity vector into a radial component (directed away from or toward the instantaneous group CoM) and a tangential component (perpendicular to the radial direction). Mean radial and absolute mean tangential velocities were averaged across all individuals at each frame.

Individual response timing heterogeneity was quantified using a cross-correlation leadership score. For each pair of individuals, the time lag at which their speed time series showed maximum cross-correlation was extracted; a negative lag indicates that the first individual tends to move before the second. The standard deviation (SD) of all pairwise lag values within a plate was used as a measure of response timing heterogeneity: a high SD

indicates that individuals responded at highly variable times, while a low SD indicates a more synchronous group response.

Principal Component Analysis

To summarise the multivariate collective behaviour profile of each plate, a plate-level PCA was performed on seven standardised summary metrics: mean pairwise Spearman r, mean pairwise distance, grid density–speed Spearman correlation, mean Moran's I, mean group polarisation, mean radial velocity, and leadership timing SD. Variables were standardised to unit variance before PCA.

Statistical Comparison Between Density Groups

All summary metrics were compared between the high-density group (P2T3, P3T3, P5T3) and the low-density group (P1T3, P6T3, P13T3) using two-sample Mann-Whitney U tests (n = 3 per group). Given the small sample size, these tests had very low statistical power, and results are reported as p-values alongside effect-size descriptions. Results are interpreted in terms of consistent directional trends and effect magnitudes rather than binary significance decisions.

Results

It is important to note that no comparison reached the conventional $p < 0.05$ threshold, consistent with the low statistical power inherent to groups of three, but several metrics show large and consistent effect sizes that are biologically meaningful and discussed accordingly.

Pairwise Speed Synchrony

For each plate, Spearman correlations were calculated for every pair of individuals and averaged to produce a mean pairwise r to quantify the degree to which individuals co-modulated their speed over time (Figure 2). High-density plates showed considerably higher pairwise correlations (P2T3: r = 0.086; P3T3: r = 0.187; P5T3: r = 0.156; group mean = 0.143, SD = 0.042) than low-density plates (P1T3: r = 0.049; P6T3: r = 0.020; P13T3: r = 0.041; group mean = 0.037, SD = 0.013; Mann-Whitney U = 9, p = 0.100). Despite not reaching a statistical significance, it can be seen that animals in high-density plates were approximately four times more synchronised in their speed fluctuations than those in low-density plates, with no overlap between groups in the upper range of plate means. The violin plots confirm that the centre of mass of the pairwise r distribution is clearly shifted positive in high-density conditions, consistent with stronger collective coupling mediated by proximity-based mechanical interaction.

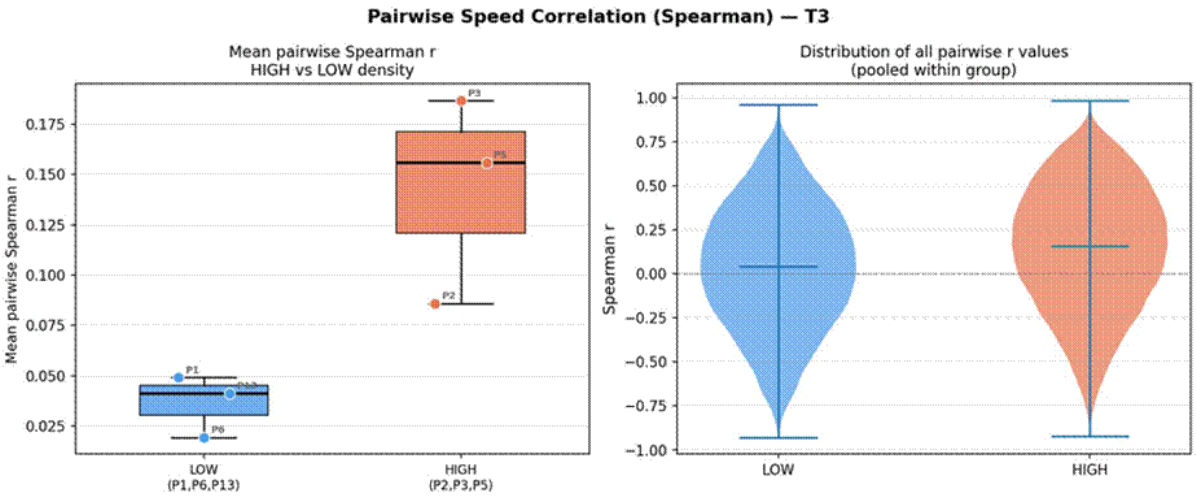

Figure 2. Pairwise speed synchrony (Spearman r). Left: box plots of mean pairwise r per plate. Right: violin plots showing the full distribution of all pairwise r values pooled within each density group. The dashed line marks r = 0. Mann-Whitney U = 9, p = 0.100.

Mean Pairwise Distance

To calculate the mean pairwise distance, mean Euclidean distances between each pair of animals were calculated per frame and averaged over the observation window (1 second) (Figure 3). High-density plates showed consistently larger mean pairwise distances (group mean = 42.2 mm, SD = 1.6 mm) than low-density plates (group mean = 37.5 mm, SD = 1.8 mm; Mann-Whitney U = 9, p = 0.100).

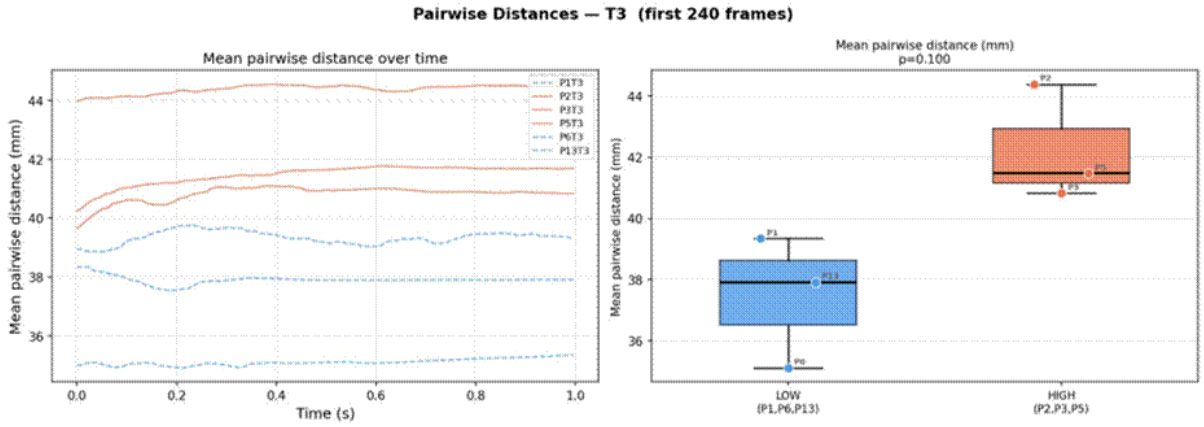

Figure 3. Mean pairwise Euclidean distance over time (left panel) and group comparison box plots (right panel). Orange solid lines = high-density plates; blue dashed lines = low-density plates. Distance values are stable across frames. Mann-Whitney U = 9, p = 0.100.

Local Density-Speed Coupling

A 5×5 spatial grid was used to compute frame-by-frame Spearman correlations between local animal density (count per cell) and local mean speed (Figure 4). A positive correlation indicated that animals in high-density sections also tended to move faster. Both groups showed consistently positive correlations throughout the recording (high density: mean r = 0.399, SD = 0.041; low density: mean r = 0.339, SD = 0.203; Mann-Whitney U = 4, p = 1.000). The absence of group difference in this metric may indicate that the local density–speed relationship is a universal property of the escape cascade mechanism. Therefore, wherever animals crowd together, physical contact or near-field vibration is more likely, thus generating a local cascade activity regardless of the plate population density.

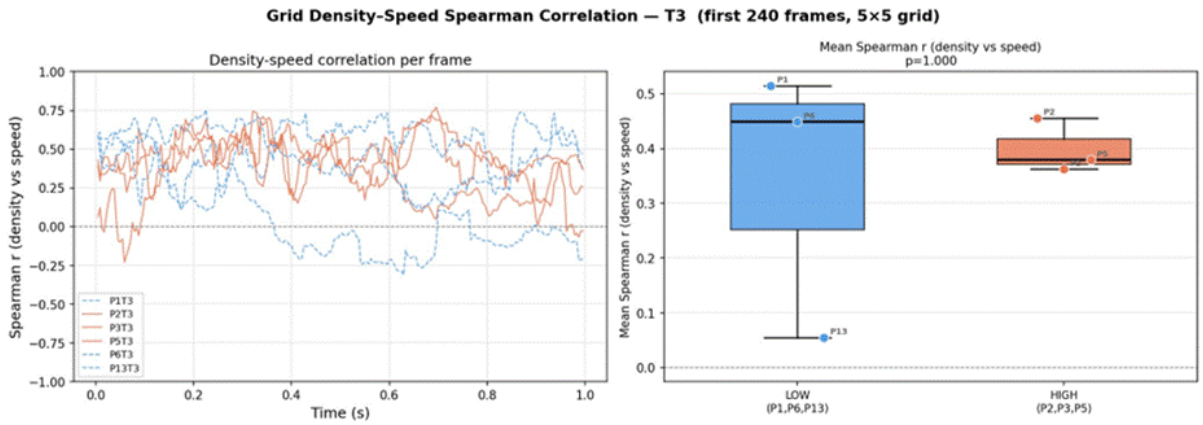

Figure 4. Grid density–speed Spearman correlation per frame (left panel) and group comparison box plots (right panel). Both groups show predominantly positive correlations throughout the recording, indicating that locally denser regions move faster in all plates. Mann-Whitney U = 4, p = 1.000.

Grid Occupancy and Spatial Distribution

Figure 5 illustrates the average distribution of animals across the arena. In the high-density group, inner dish cells contained between 10 and 35 animals per frame on average, with the highest concentrations in the lower-central region (grid rows 2–3, columns 2–4). The low-density group showed far lower absolute occupancy (2–14 animals per cell) with a more skewed distribution biased toward the right and lower-right sectors of the dish. This spatial asymmetry is replicated to varying degrees across all plates.

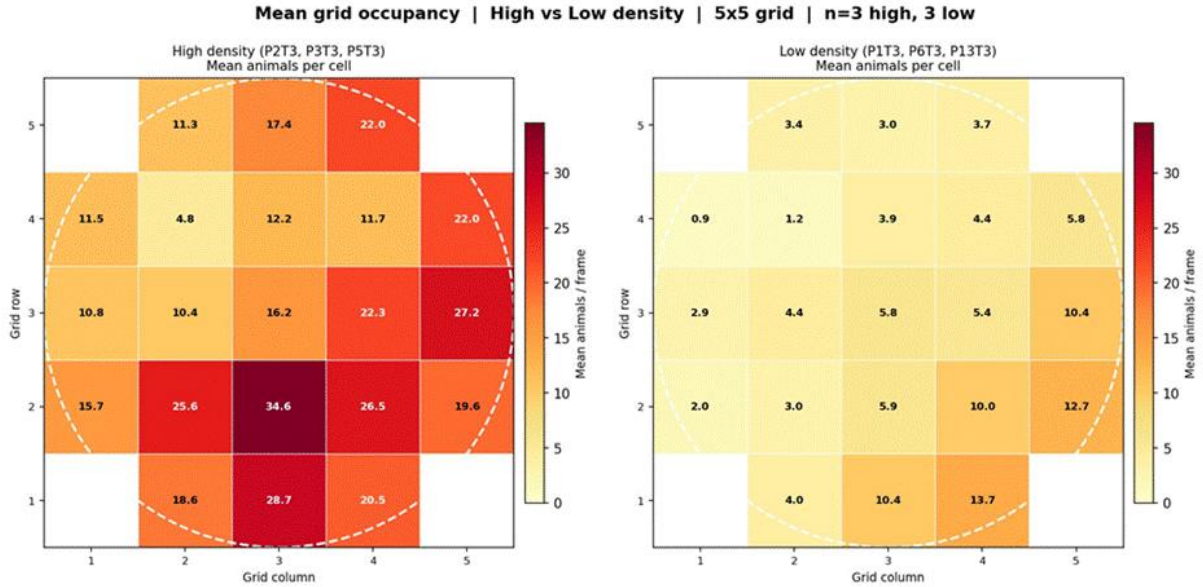

Figure 5. Mean grid occupancy per cell (5×5 grid), averaged across plates within each density group. Cell values indicate the mean number of animals per frame. White cells fall outside the dish boundary. Left: high-density group. Right: low-density group. The dashed circle marks the dish perimeter.

Moran's I: Spatial Autocorrelation of Speed

Moran's I per frame was calculated across all plates to determine whether spatially adjacent individuals moved at similar speeds (neighbourhood threshold 13mm=150px) (Figure 6). All plates yielded mean Moran's I value above zero (high density: mean = 0.022, SD = 0.016; low density: mean = 0.034, SD = 0.031; Mann-Whitney U = 4, p = 1.000), which confirms a consistent positive spatial autocorrelation of speed across all plates: fast animals clustered near other fast animals more than expected under spatial randomness.

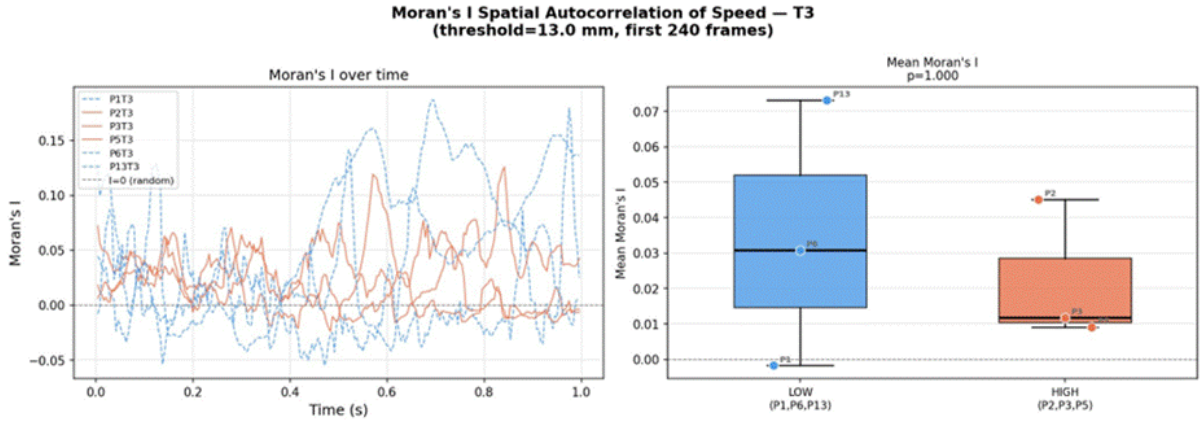

Figure 6. Moran's I spatial autocorrelation of speed over time (left panel) and group comparison box plots (right panel). Neighbourhood threshold = 13.0 mm. Mann-Whitney U = 4, p = 1.000.

Kinematics of the Escape Response

The collective escape response following disturbance is characterised by the temporal profile of mean population speed (Figures 7 and 8). All plates exhibited a sharp initial speed peak in the first 0.1 seconds, consistent with the mechanical trigger of lid removal. At the group level (Figure 8), high-density plates reached a peak mean speed of 51.65 mm/s at t = 0.071 s, marginally earlier than low-density plates (50.63 mm/s at t = 0.096 s), suggesting a slightly faster collective response in high-density conditions. The most significant distinction was in the post-peak trajectory: high-density plates decayed to a low, stable residual speed (3.78 mm/s), while low-density plates maintained a higher and more variable residual activity (7.20 mm/s). This sustained low-density activity was driven almost entirely by P1T3 (mean speed = 29.13 mm/s; peak = 118.81 mm/s), which showed repeated secondary bursts throughout the full second of recording, indicating ongoing escape cascades well beyond the initial startle. The standard deviation at peak was higher for low-density plates (48.25 mm/s vs. 38.12 mm/s), reflecting a bigger inter-plate variability in escape response.

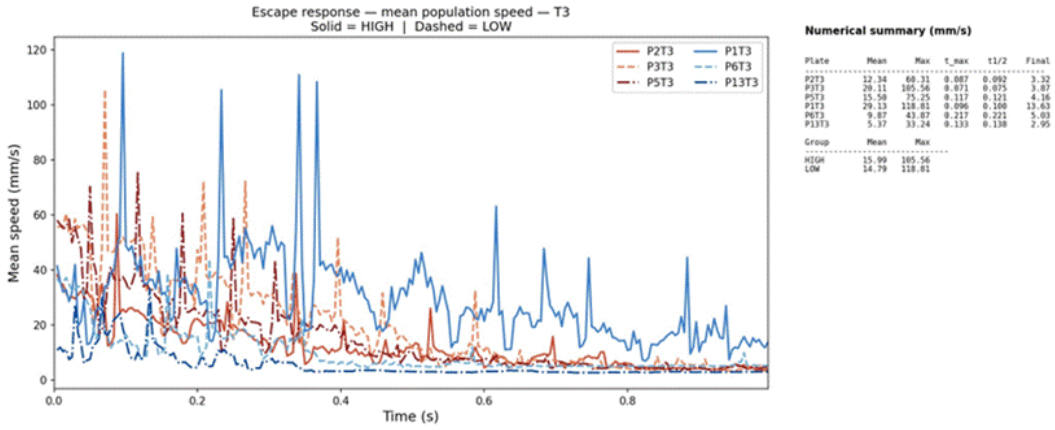

Figure 7. Escape response for all six plates. Mean population speed over 240 frames (one second). Solid lines = high-density plates; dashed lines = low-density plates. The numerical summary table reports per-plate mean speed, peak speed, time to peak (t_max), half-peak decay time (t1/2), and final speed.

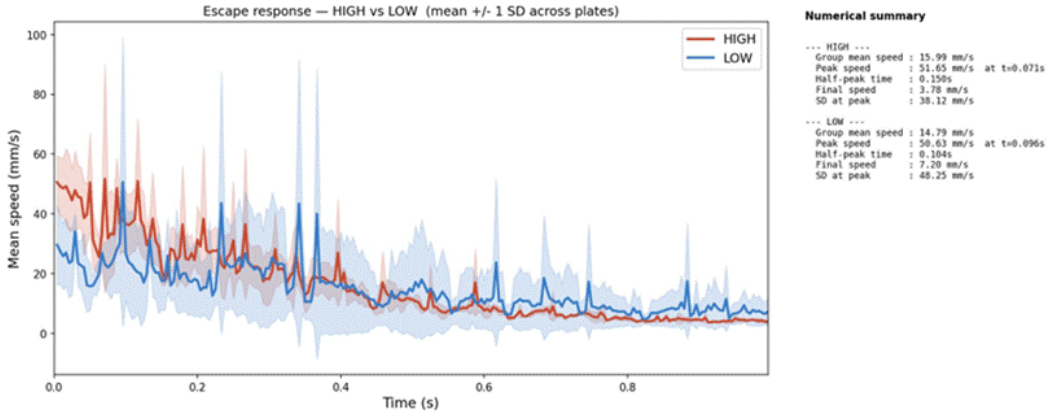

Figure 8. Group-level escape response. Lines show group mean speed; shaded regions = ±1 SD across plates within each group. High-density plates (orange) show a marginally earlier peak and lower, more uniform residual speed. Low-density plates (blue) show greater inter-plate variability and sustained secondary activity.

Centre of Mass Displacement

Centre of mass displacement (CoM) is the measure of the net group-level displacement from the initial position at t = 0 (Figure 9). High-density plates showed substantially smaller CoM displacements throughout the recording (group mean = 0.47 mm, maximum = 1.12 mm) compared to low-density plates (group mean = 0.97 mm, maximum = 2.63 mm). All three high-density plates stabilised below 0.55 mm by t = 0.3 s.

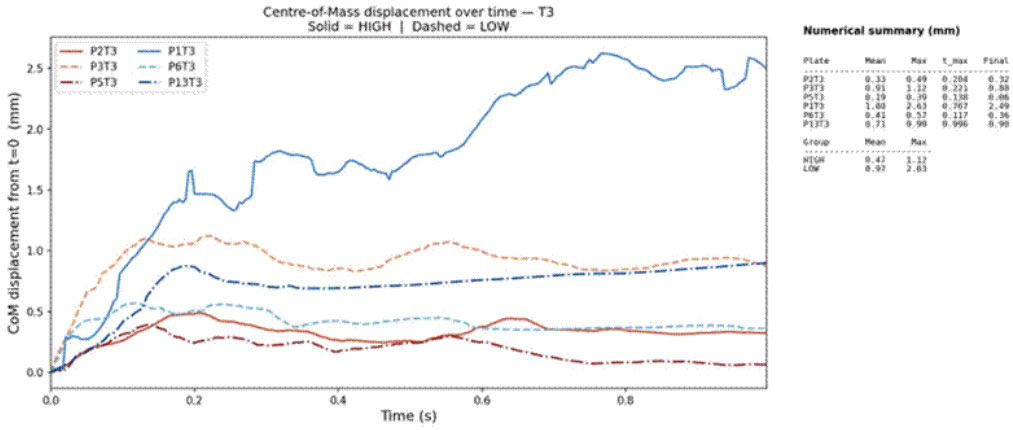

Figure 9. Centre-of-mass displacement from t = 0 over 240 frames. Solid lines = high-density plates; dashed lines = low-density plates. P1T3 (solid blue) shows the largest and most sustained displacement of any plate. The numerical summary reports per-plate mean, maximum, time of maximum, and final displacement.

Directional Order: Polarisation and Heading Distribution

Group polarisation Φ(t) is the magnitude of the mean unit heading vector and quantifies the degree to which animals move in a shared direction (Figure 10). Φ(t) was extremely low for both density groups throughout the observation window (High density: mean Φ = 0.052, SD = 0.028; Low density: mean Φ = 0.078, SD = 0.045; Mann-Whitney U = 2, p = 0.400).

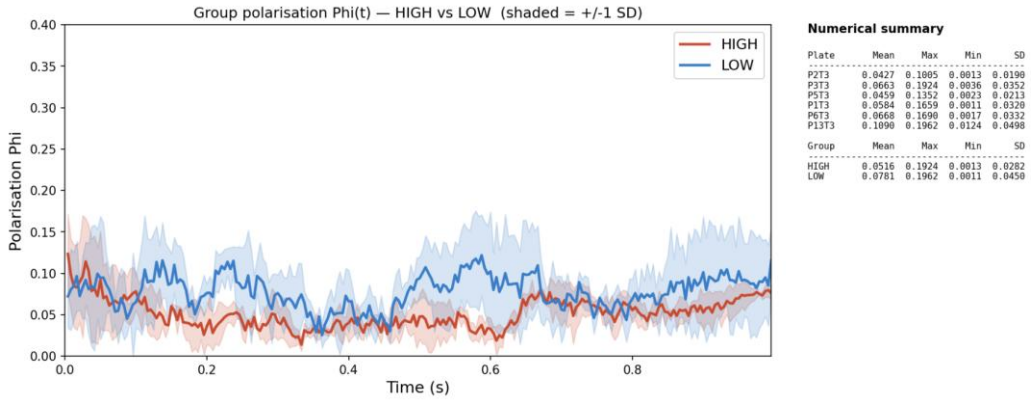

Figure 10. Group polarisation Φ(t) over time. Lines show group means; shaded regions = ±1 SD. Y-axis fixed at 0–0.40. Both groups remain far below meaningful directional alignment thresholds throughout the recording. The numerical summary reports per-plate and per-group mean, maximum, minimum, and SD of Φ. Mann-Whitney U = 2, p = 0.400.

Additionally, heading rose plots (Figure 11) also confirm the absence of directional preference. Animal movement directions were broadly distributed across all 360°, with a notable excess at approximately 0° (east) in both density conditions.

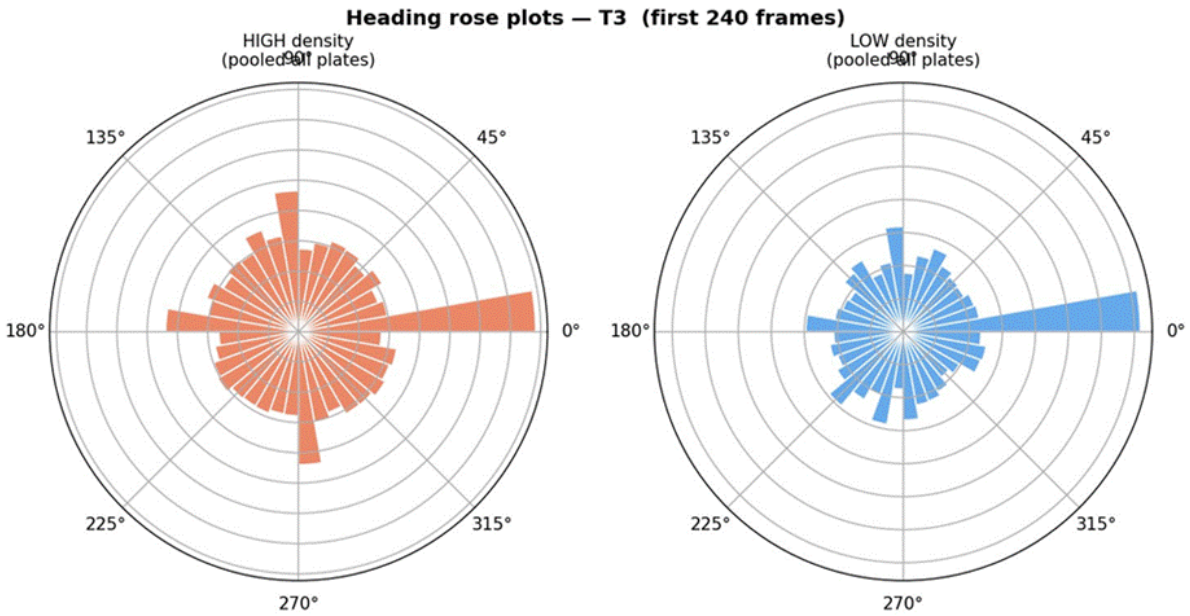

Figure 11. Heading rose plots for high-density (orange, left) and low-density (blue, right) groups, pooled across all plates within each group. Radial extent indicates relative frequency. Both groups show broadly uniform distributions with a shared eastward (0°) bias likely attributable to a systematic experimental asymmetry.

Vector analysis of Radial and Tangential Velocity Components

Decomposing individual velocities into radial (centrifugal/centripetal) and tangential (rotational) components relative to the instantaneous group CoM reveals the geometric structure of the escape response (Figure 12). At t = 0, high-density animals showed a strong positive mean radial velocity of approximately +8.5 mm/s, indicating rapid centrifugal expansion away from the group centre. However, this rapid burst decayed to almost zero in just 0.3 seconds. Low-density animals showed a mildly negative radial velocity at onset (≈ −2.5 mm/s), suggesting slight initial inward movement before decreasing toward zero. Tangential velocity was significantly higher in high-density plates at the beginning (≈29 mm/s vs. ≈14 mm/s for low density). Both components decreased to near zero in 0.6 seconds.

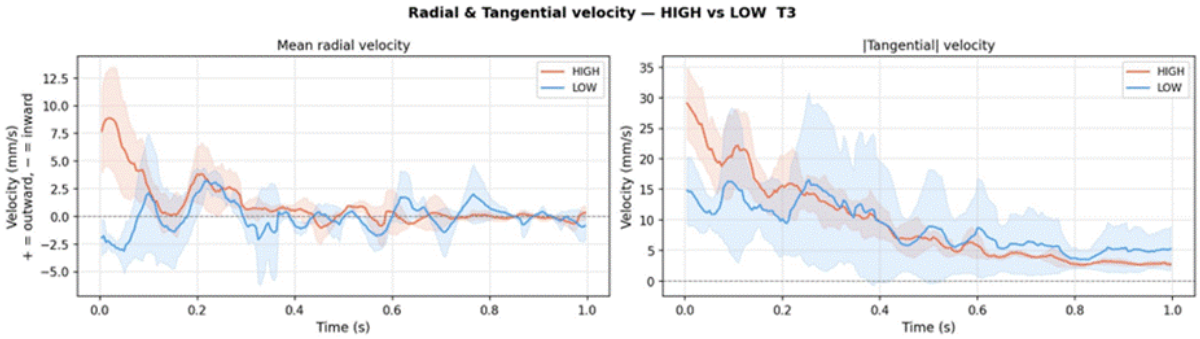

Figure 12. Radial velocity (left panel) and absolute tangential velocity (right panel) relative to the group CoM. High density = orange; low density = blue. Shaded regions = ±1 SD. Positive radial velocity indicates outward movement from the group centre. High-density plates show a stronger initial centrifugal burst and higher tangential speeds.

Heterogeneity of the Individual Response: Leadership Timing

An index of heterogeneity in response timing was the standard deviation (SD) of cross-correlation-derived leadership scores across individuals within each plate (Figure 13). A higher leadership SD indicates more variable response timing, while a lower SD indicates more synchronous collective response. Low-density plates showed a more clustered and higher leadership SDs (P1T3: 179.5 ms; P6T3: 184.8 ms; P13T3: 183.7 ms; group mean = 182.7 ms, SD = 2.3 ms), thus indicating a more heterogeneous response timing in every low-density plate. Contrarily, high-density plates showed a lower mean leadership SD (group mean = 172.4 ms, SD = 9.1 ms) but with far greater inter-plate variability (Mann-Whitney U = 2, p = 0.400). P5T3 achieved the lowest leadership SD of any plate (162.4 ms across 470 individuals), indicating near-synchronous cascading responses, while P2T3 was as heterogeneous as the low-density group (184.4 ms).

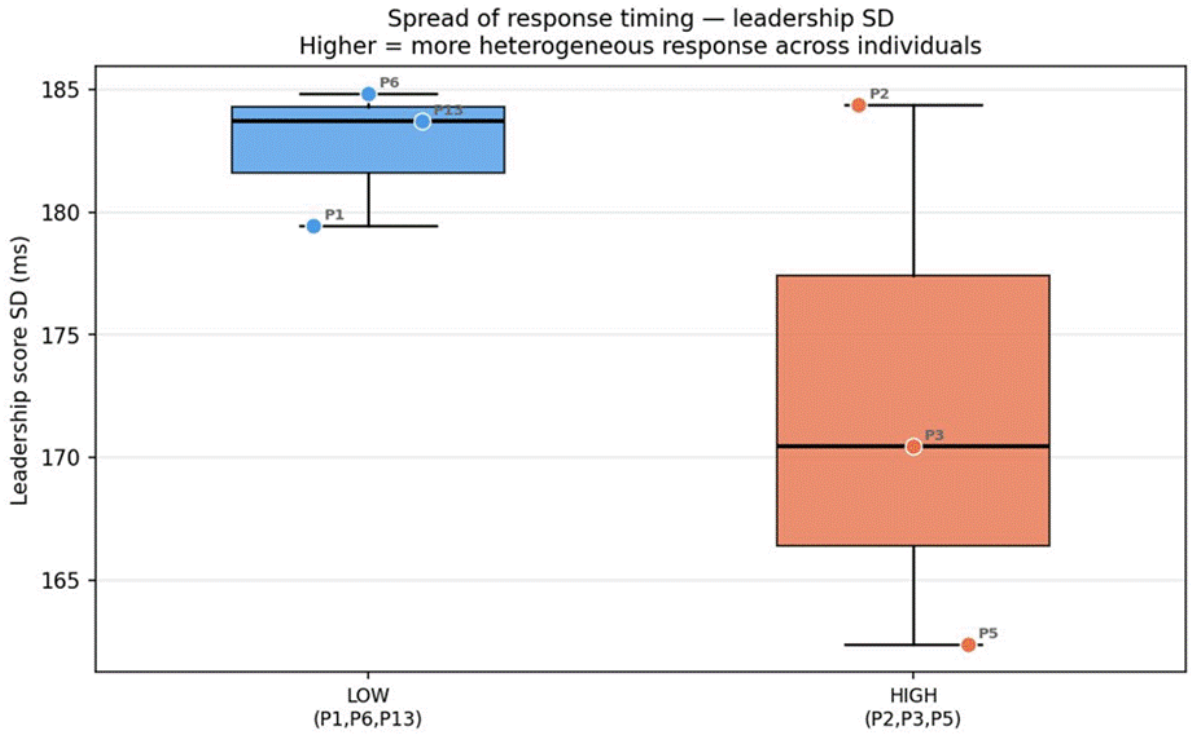

Figure 13. Spread of individual response timing (leadership score SD) per plate, grouped by density condition. Higher values indicate more heterogeneous response timing. Individual plate values are annotated; open circles show group medians. Low-density plates show consistently high and tightly clustered leadership SD. High-density plates show greater inter-plate variability. Mann-Whitney U = 2, p = 0.400.

Spatial Speed Distribution

Figures 14 and 15 show the mean speed of animals passing through each other in a 5x5 grid, averaged over 240 frames (1 second). Individual plate maps (Figure 14) reveal that high-density plates displayed relatively uniform, moderate mean cell speeds across the dish interior

(range: 4.6–28.6 mm/s). In comparison, low-density plates showed wider within-plate variation, with several extremely high-speed cells notably in P1T3 (column 2, row 4: 104.4 mm/s; column 2, row 2: 76.4 mm/s). These values are explained by the fact that in plates with few animals, cells with very low visitation rates will have their average dominated by individual high-speed jump events.

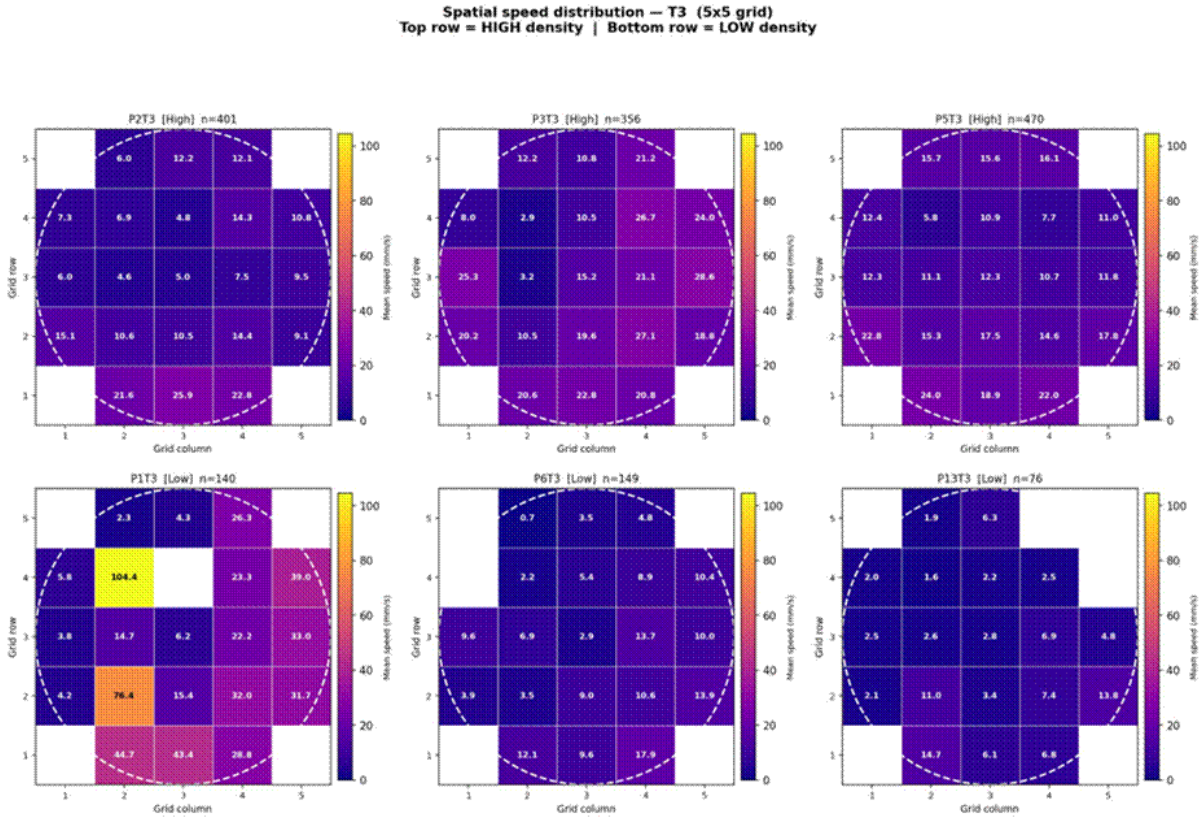

Figure 14. Spatial speed distribution for all six plates (5×5 grid). Cell values indicate mean speed (mm/s) averaged over 240 frames. The colour scale is shared across all panels (0–100 mm/s). Top row = high density; bottom row = low density. White sections in low-density plates indicate the grids which did not receive enough animal visits to calculate a mean speed.

When speed maps were averaged across plates within each density group (Figure 15), the high-density group showed a spatially homogeneous speed field (in-dish cell range: 5.2–22.5 mm/s), consistent with uniform arena coverage and distributed escape activity. The low-density group displayed a less uniform distribution with two prominent high-speed regions at grid positions (columns 1–2, rows 2 and 4) reaching 23.8–36.1 mm/s. However, this pattern is largely attributable to P1T3 alone; the remaining two low-density plates showed spatially distributed speed fields comparable to those of the high-density group. The averaged low-density speed map should therefore be interpreted with caution, as it does not represent a consistent group-level pattern but instead reflects the disproportionate influence of a single plate.

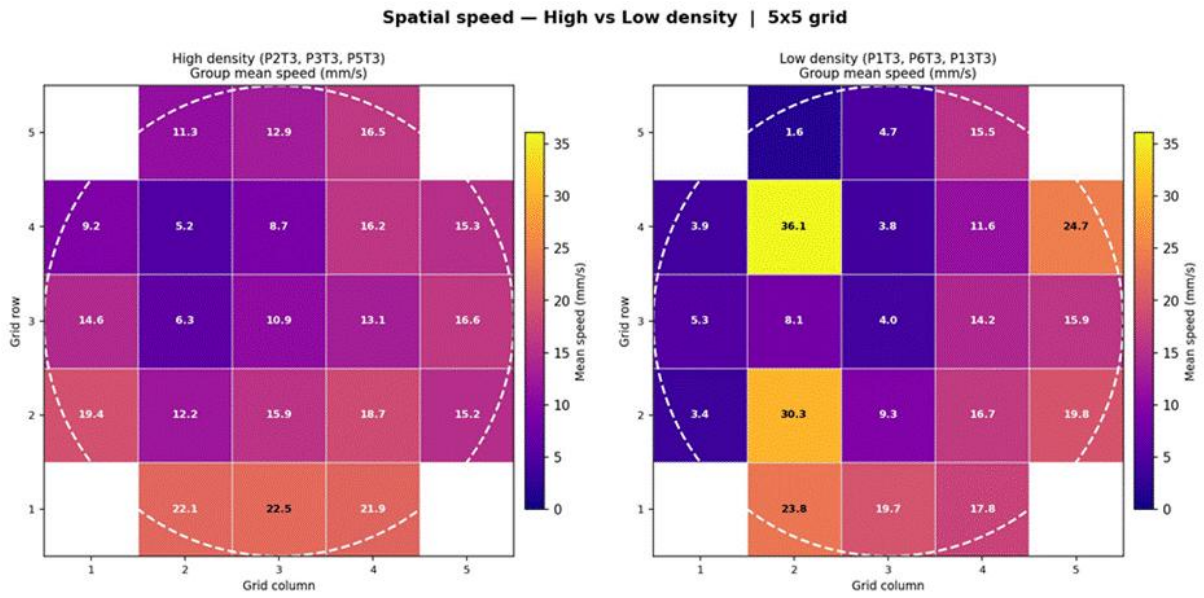

Figure 15. Group-mean spatial speed maps for high-density (left) and low-density (right) groups. Cell values show the mean speed (mm/s) averaged across all plates in each group. White cells fall outside the dish boundary. The dashed circle marks the dish perimeter.

Spatial Behavioural Speed Correlation

Spearman correlations were computed between the spatial distance separating each pair of animals (based on mean positions) and their behavioural distance (1 − Spearman r), to test whether spatial proximity predicted speed synchrony (Figure 16). Five of the six plates showed small but statistically significant positive correlations: P2T3 ($r = 0.046$, $p < 0.001$), P3T3 ($r = 0.070$, $p < 0.001$), P1T3 ($r = 0.034$, $p < 0.001$), P6T3 ($r = 0.036$, $p < 0.001$), and P13T3 ($r = 0.082$, $p < 0.001$). P5T3 was the only exception with $r = -0.004$, $p = 0.172$, showing no spatial–behavioural relationship. Despite their statistical significance, achievable because of the large number of pairs analysed, effect sizes were uniformly weak across all plates ($r < 0.10$), indicating that spatial distance explains only a very small proportion of variance in speed synchrony.

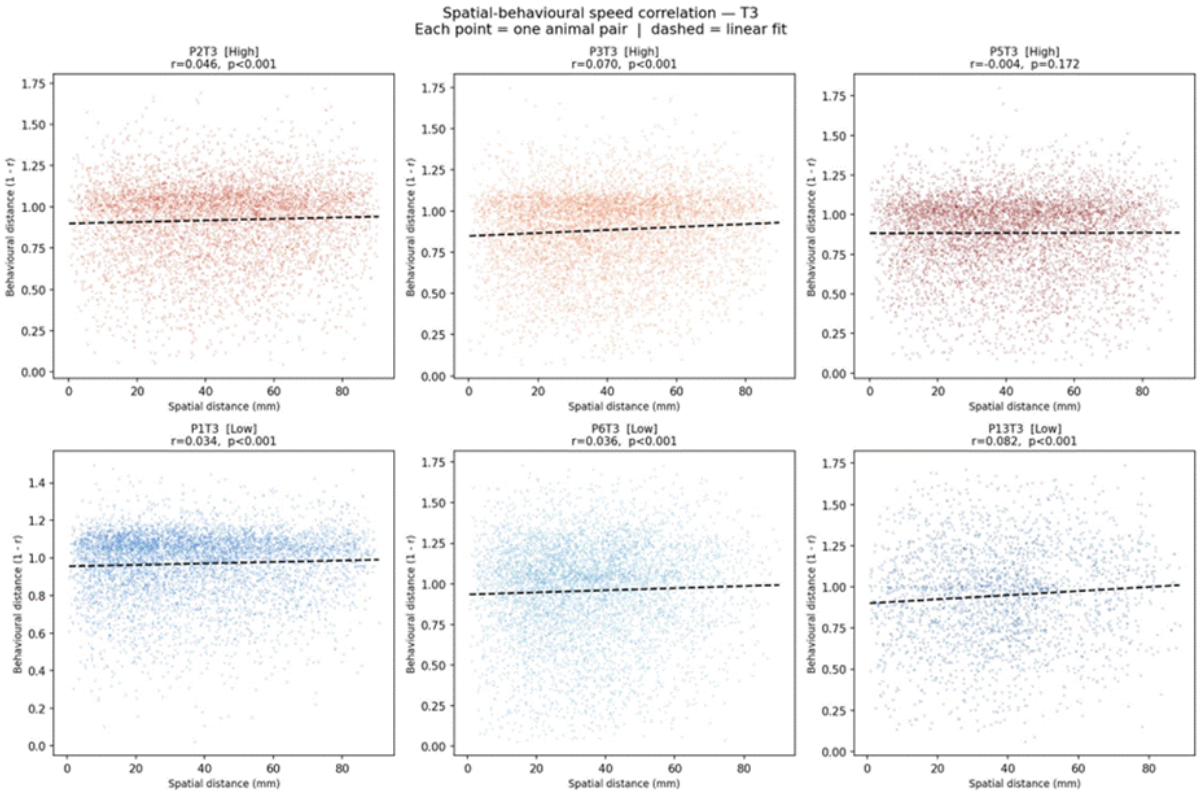

Figure 16. Spatial–behavioural speed correlation for all six plates. Each point represents one animal pair; x-axis = spatial distance between mean positions (mm); y-axis = behavioural distance (1 − Spearman r). Dashed lines show linear fits. Spearman r and p-values are annotated per panel. Top row = high density; bottom row = low density.

Principal Component Analysis

A principal component analysis (PCA) was performed on standardised values of mean pairwise speed correlation, mean pairwise distance, grid density–speed correlation, Moran's I, group polarisation, mean radial velocity, and leadership timing SD. The scree plot (Figure 17) shows that PC1 captured 59.3% of total variance and PC2 a further 22.1%, meaning that 81.4% of the multivariate structure across plates was accounted for by the first two components alone. An additional component was needed to reach 95% of cumulative variance.

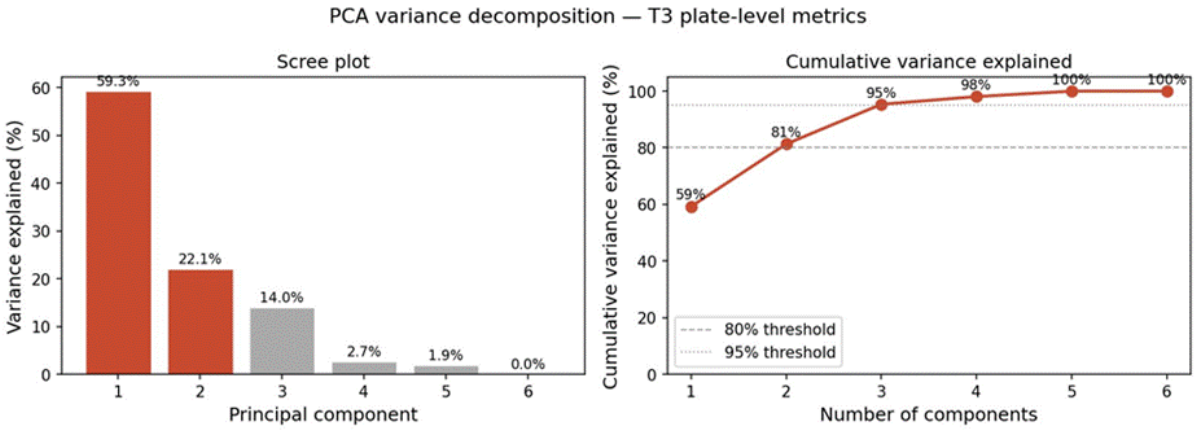

Figure 17. PCA variance decomposition. Left: scree plot showing the percentage of total variance explained by each principal component. PC1 and PC2 (highlighted in orange) together account for 81.4% of the variance. Right: cumulative variance explained as a function of the number of components retained, with 80% and 95% threshold lines for reference.

PC1's highest positive loadings were on radial velocity (+0.46), pairwise speed synchrony (+0.39), and pairwise distance (+0.29), while its strongest negative loadings fell on Moran's I (−0.39), group polarisation (−0.39), and leadership timing SD (−0.39). Plates with high PC1 scores combined a strong inter-individual speed synchrony and explosive outward escape bursts with lower spatial autocorrelation and more homogeneous response timing.

The PC1 and PC2 scores per plate are shown in Figure 18. On PC1, the high-density plates P3T3 (1.84) and P5T3 (2.51) scored substantially higher than all low-density plates (P6T3: −1.42; P13T3: −3.60), with their group means falling clearly on opposite sides of zero (HIGH mean = +1.57; LOW mean = −1.57). This confirms that the high-density condition systematically shifts the collective behaviour profile toward stronger coupling along the primary axis of multivariate variation. However, two plates did not follow this pattern: P1T3 (Low density, n = 140) and P2T3 (High density, n = 401) both scored near zero on PC1 (0.33 and 0.35, respectively), lying between the two density groups rather than within them. For P1T3, this can be explained by its unusually active escape profile, characterised by persistent secondary speed bursts and the largest CoM displacement of any plate. While for P2T3, it can be explained by its weak synchrony in comparison to the other two plates from the high-density treatment.

On PC2, the pattern was less structured: both density groups contained plates with positive and negative scores, and group means were symmetric at ±0.44. This confirms that the secondary axis of variation, which contrasts local density–speed coupling against overall synchrony, is not systematically related to density.

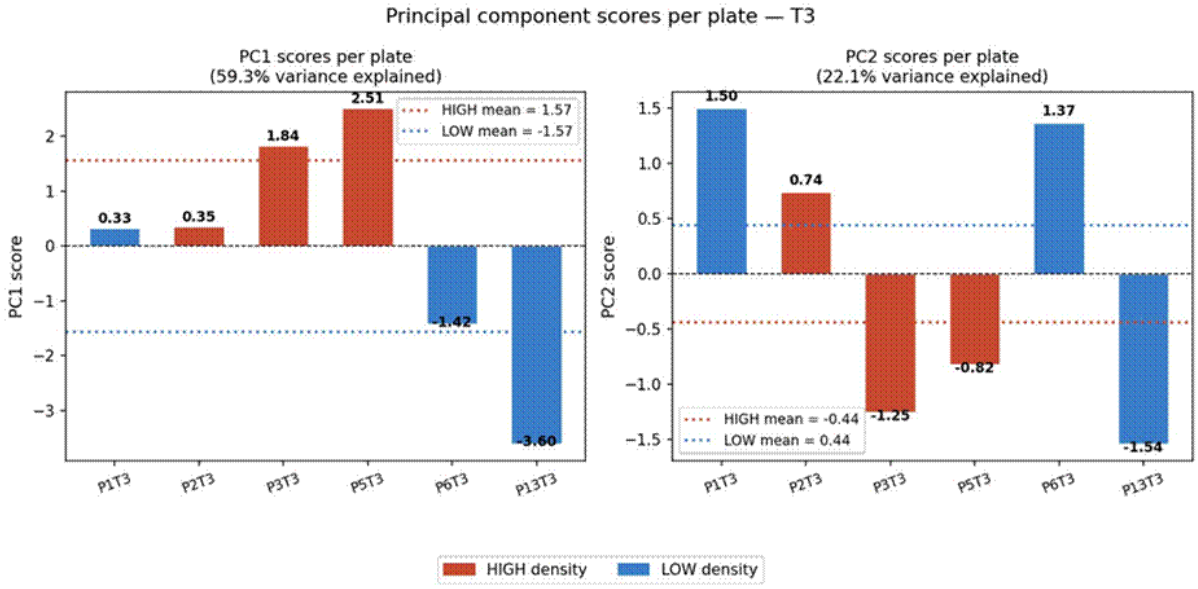

Figure 18. Principal component scores per plate for PC1 (left, 59.3% variance) and PC2 (right, 22.1% variance). Orange bars = high-density plates (P2T3, P3T3, P5T3); blue bars = low-density plates (P1T3, P6T3, P13T3). Dotted lines indicate the group mean score for each density condition. On PC1, high-density plates score consistently positive and low-density plates consistently negative, with the exception of P1T3 and P2T3, which both score near zero. PC2 shows no density-related pattern.

Discussion

The aim of this study was to investigate whether population density influenced the collective escape response dynamics in springtails. Across twelve quantitative metrics and multivariate PCA, a somewhat consistent pattern emerged: high-density groups exhibited stronger temporal speed synchrony, more explosive and geometrically organised initial escape bursts, and smaller net centre-of-mass displacement, while low-density groups showed greater spatial heterogeneity in activity and more sustained, individualised escape behaviour. The following sections interpret these findings and compare them to empirical studies of other collectively moving species, and examine the constraints that limited the strength of interference from the present dataset.

Density as a Coupling Parameter: Parallels with Self-Propelled Particle Models

The most important theoretical framework that can be used to interpret these results is the self-propelled particle (SPP) model introduced by Vicsek and Zafaeiris (2012) which predicts a phase transition from disordered to ordered collective motion as particle density increases above a critical threshold. In the original model, density and noise are the two primary parameters controlling the order parameter φ (the degree of directional alignment) and collective order emerges only when the density of locally interacting particles is sufficient for alignment information to propagate across the group. The present results suggest that density may act as a coupling parameter in springtails, but reveal that the order it generates might be of a qualitatively different kind: it is temporal synchrony of speed, not directional alignment. In the Vicsek model, interactions are realized by the alignment of velocities within a neighbourhood radius. However, springtails seem to have no practical mechanism for velocity alignment: they do not sense a neighbour's movement direction and align to it, nor do they follow visual or acoustic cues in real time. Their interaction is presumably mechanical – a jumping animal displaces air and substrate, physically disturbing its neighbours within a short radius, and triggering their own escape jump independently of direction. The springtail escape cascade is probably more accurately modelled as a contagion process on a proximity graph, like the escape wave models for locust marching bands (Ariel and Ayali, 2015), rather than as a velocity-alignment process. In such models, the main role of density is to increase the connectivity of the interaction graph: as density increases, each individual has more neighbours within its trigger radius simultaneously and the probability that a local escape event propagates

to the whole group increases. The four-fold increase in pairwise speed synchrony found here is broadly consistent with this connectivity-driven coupling model.

The lack of directional order at any density is consistent with qualitative predictions of escape-only SPP models (Romanczuk et al., 2009), where individual escape behaviour leads to local speed homogenisation but not to global directional order, because the escape directions are random with respect to the group. Whether a sufficiently extreme increase in density could drive a transition to directional order in springtails is an open empirical question. For locusts, their density drives the transition from disordered hopping to coordinated marching (Buhl et al., 2006). The present experimental design cannot address this question.

Speed Synchrony Without Directional Alignment: A Distinct Form of Collective Behaviour

The difference between high pairwise speed synchrony in high density plates and identical group polarisation across both conditions positively characterizes the type of collective behaviour springtails exhibit. This form of collective dynamics, where timing and intensity of individual activity are coordinated without any directional order, has been described as amplitude synchrony and may be considered analogous to syncrhonized alarm responses in bird flocks where multiple individuals respond to one predator simultaneously but without aligning their flight directions (Couzin, 2009).

The weak trend of relatively high polarisation values in low-density plates (mean Φ = 0.078 vs. 0.052) should not be interpreted as evidence for greater directional coordination in smaller groups. This pattern is only consistent because of small-N statistical bias in polarisation metrics, where smaller groups tend to produce more incidental directional correlations by chance, even in the absence of any true alignment tendency. Considering that low-density plates contained significantly less individuals per arena, this alone may be sufficient to explain the observed difference, and any behavioural interpretation of the polarisation difference between high vs low density conditions should be made with caution

The spatial–behavioural correlation analysis provides mechanistic insight into how this synchrony is generated. Five of the six plates showed a statistically significant positive relationship between spatial proximity and speed synchrony, confirming that the coupling is contact- or proximity-mediated rather than long-range. Importantly, this effect was absent in P5T3 (n = 470), the densest plate, where spatial distance explained no variance in synchrony. This is because at very high densities, all individuals are simultaneously within triggering range of enough neighbours, therefore, the spatial distance gradient becomes irrelevant. This pattern parallels the ‘all-to-all’ coupling regime described by Bode et al. (2011), where interaction

network homogeneity beyond a critical threshold no longer further increases collective cohesion, and suggests that P5T3 may be near or above a connectivity saturation threshold for this system.

The Moran's I spatial autocorrelation analysis adds another distinction to this characterisation. While density did elevate the temporal synchrony of speed fluctuations between individuals, it did not increase the spatial clustering of fast-moving animals at any given moment, because mean Moran's I values were statistically indistinguishable between high- and low-density plates (mean = 0.022 vs. 0.034, Mann-Whitney U = 4, p = 1.000). This dissociation may suggest that density primarily amplifies the temporal coordination of the escape response (when animals respond) rather than concentrating activity spatially into particular regions of the arena. Combined with the absence of directional alignment, this positions the springtail escape cascade as a system in which density tightens the timing of individual responses across the group without reorganising their spatial structure.

Escape Kinematics and Centre-of-Mass Geometry

The marginally earlier speed peak seen in high-density plates (t = 0.071 s vs. 0.096 s) and the lower, more stable residual speed are consistent with faster cascade propagation and a more complete group-level response: when animals are densely packed, the disturbance spreads more rapidly, thus producing a sharper and more synchronous activity peak, after which activity subsides because fewer individuals remain untriggered. In contrast, low-density plates showed more sustained secondary activity, most dramatically in P1T3, which maintained high mean speed with repeated bursts throughout the full second of recording, consistent with a lower per-individual coupling probability, leaving subsets of animals triggered later or repeatedly.

The centre-of-mass (CoM) displacement results provide perhaps the most intuitive visualisation of the density effect. Low-density plates showed substantially larger and more persistent CoM displacement (mean maximum 2.63 mm vs. 1.12 mm), driven predominantly by P1T3. This reflects the asymmetric spatial distribution of animals in low-density plates: when animals cluster in one sector of the dish, a wave of escape jumps propagates through that sector with insufficient counteracting activity elsewhere to cancel the net displacement. High-density plates, filling the arena more uniformly, produced a centrifugally symmetric escape burst, which was confirmed directly by the radial velocity analysis, that largely cancels at the group level.

The radial velocity decomposition further revealed that low-density animals showed a slight inward convergence at response onset (≈ −2.5 mm/s), likely reflecting their clustering in one sector of the dish at the moment of disturbance: animals on the inner edge of the cluster

initially jump toward the group centre before the outward cascade dominates. The higher tangential velocity in high-density plates at burst onset (≈29 mm/s vs. ≈14 mm/s) reflects the greater absolute speeds generated during the initial escape rather than any rotational organisation, as both components decayed to near zero within 0.6 seconds, which is consistent with the escape response being a transient burst rather than a sustained collective motion. This suggests an ecological implication: a high-density aggregation may be collectively harder to dislodge from a location under natural predation pressure, not because individuals jump less, but because they jump more symmetrically.

Leadership Timing and Response Propagation

The leadership SD analysis revealed that low-density plates showed consistently high and tightly clustered leadership SDs (group mean = 182.7 ms, SD = 2.3 ms), indicating consistently heterogeneous response timing. High-density plates showed a lower mean but greater inter-plate variance (mean = 172.4 ms, SD = 9.1 ms), with P5T3 achieving near-synchronous responses (162.4 ms) while P2T3 was as heterogeneous as any low-density plate (184.4 ms). This divergence seen in the high-density plates suggests that density alone does not determine propagation structure. Instead, it is likely that the spatial configuration of animals relative to the epicentre of the disturbance at the moment of stimulus significantly modulated escape response dynamics. This parallels with findings described by Nagy et al. (2010), who demonstrated that leadership hierarchies in pigeon flocks were context-dependent, with leading positions shifting based on the spatial structure of the group at the time of a direction change.

It is important to note that springtails presumably do not have the capacity for individual recognition, hence the leadership in springtails almost certainly does not reflect social dominance or individual trait differences. Any detected response sequence is more likely attributed to spatial positioning and the physical geometry of disturbance propagation. Therefore, the leadership SD metric is best interpreted as a measure of group-level response synchrony rather than evidence for consistent leader-follower relationships.

Methodological Limitations

The interpretation of all results must be qualified by a set of methodological limitations that constrain the strength of inference achievable from the current dataset.

The most fundamental limitation is the sample size of three plates per density group. This was insufficient to achieve statistical significance in any of the analysed metrics, despite several showing biologically large effect sizes. This situation arose from a combination of factors. Firstly, manual annotation of individual springtail trajectories in CVAT is extremely time-

consuming: high-density plates with 400–470 individuals required approximately 60–70 hours of human annotation time per plate. Given this constraint, only a limited number of plates could be fully processed within the project timeline. Another issue occurred with the CVAT annotation software itself, where some of the annotated points got lost due to technical issues, which resulted in high population variance between different trials of the same plates. This reduced the comparability of data across sessions and resulted in exclusion of data from Trial 2 entirely. Therefore, the current results should be treated only as preliminary, requiring replication with a larger number of plates per condition before any observed trends can be considered confirmed.

A further issue related to the CVAT annotation workflow was concerning the behavior of the software's built-in semi-automatic tracker. CVAT has a tracking algorithm which is designed to predict the position of an annotated object in subsequent frames based on its prior trajectory. While this feature is intended to fasten the annotation process, it introduced a serious issue in the springtail context: since springtail movement between frames can often be rapid, discontinuous, and unpredictable, the tracker often misidentified the predicted position of an individual after a jump. This required manual correction by the annotator, and in cases where it did not, the tracker would continue propagating a position estimate based on the pre-jump trajectory. This might have produced artificially smooth trajectory segments between manually verified positions, thus potentially attenuating the true speed peaks in individual tracks and introducing noise into all metrics derived from positional data. It is difficult to quantify the extent of this error, as it depended on the attentiveness of the annotator.

Another limitation is regarding the standardisation of the disturbance stimulus. The escape response was triggered by the manual removal of the petri dish lid. While the action was performed consistently and carefully by the same individual through all recordings, the speed, the angle, and precise timing could not be perfectly controlled. As a result, it is possible that the mechanical vibration transmitted to the dish and the animals' reaction to it subtly varied between trials. This variation is impossible to quantify retrospectively and may have contributed to inter-plate variability in response magnitude and timing, particularly in the initial speed peak, where the time to peak group mean speed (t_max) ranged from 0.071 to 0.217 s across plates. To eliminate this variability, it is recommended to recreate this study with an automated, electrically triggered disturbance mechanism.

Moreover, in the heading distribution data, rose plots revealed a shared excess of eastward-directed movement (approximately 0°) across both density conditions, which cannot reflect a genuine behavioural preference given its consistency across independent plates. This bias is almost likely explained by the asymmetry in the experimental setup, including the

illumination source, direction of the lid removal, and camera positioning relative to the arena placement. Future recordings should standardise lighting symmetrically around the arena and ensure the disturbance stimulus is delivered without a directional component, so that heading distributions can be interpreted as purely behavioural rather than partly apparatus-driven.

Finally, the one second recording window captures only the immediate response and its initial decay. The long-term dynamics, including return to baseline activity and spatial redistribution were not captured in this study. Extending both the number of plates and the length of recordings would allow characterisation of the full temporal profile and its aftermath more precisely.

One additional geometric caveat concerns the mean pairwise distance metric. The larger mean pairwise distances observed in high-density plates (group mean = 42.2 mm) compared to low-density plates (group mean = 37.5 mm) reflect a geometric consequence of space filling rather than a behavioural signal. As animal number increases within a fixed arena, individuals distributed across the full dish will on average be further apart from any randomly selected pair than a smaller group that tends to occupy only a subsection of the available space. Accordingly, mean pairwise distance in this context serves better as a descriptor of spatial spread than as a direct index of social cohesion or avoidance, and should be interpreted with this constraint in mind.

Future work should prioritise three improvements. First, sample size must be increased substantially: a minimum of eight to ten plates per density condition is recommended to achieve adequate statistical power for the effect sizes observed here. Second, the disturbance stimulus should be standardised using an automated mechanical delivery system to eliminate inter-trial variability in stimulus characteristics. Third, and most critically for scaling to the required sample sizes, manual annotation should be replaced or substantially assisted by automated tracking. Computer vision and machine learning approaches, including multi-object tracking frameworks such as SORT and DeepSORT, or purpose-built animal tracking tools can offer a realistic path to semi-automated or fully automated annotation. A deep learning model trained on a subset of manually annotated springtail frames could potentially reduce annotation time from 60 hours to minutes per plate, making the sample sizes required for statistically robust inference practically achievable within a standard research timeline.

Strengths of the Analytical Framework

Despite the limitations mentioned above, the analytical framework developed throughout this study still represents a substantial methodological contribution. The multi-metric approach: integrating pairwise speed synchrony, spatial autocorrelation, grid-based density and speed

mapping, radial and tangential velocity decomposition, polarisation, CoM displacement, leadership timing, spatial–behavioural correlation, and multivariate PCA, provides a comprehensive characterisation of collective dynamics that goes considerably beyond the single-metric approaches common in invertebrate collective behaviour research. The Python analysis pipeline developed for this project is fully modular and reproducible. With modifications to the plate configuration, the same pipeline can be applied immediately to any number of additional recordings, making it straightforward to expand the dataset without redesigning the analysis.

Broader Implications

Springtails are among the most abundant terrestrial arthropods, with population densities in soil litter regularly exceeding tens of thousands of individuals per square metre (Hopkin, 1997). Despite this ecological significance, the collective dynamics of their escape responses had received no quantitative treatment in the literature prior to the present study. The demonstration that density modulates coupling strength and geometric organisation of the escape response provides a foundation for understanding how springtail groups function as collective units under natural predation pressure. From the perspective of collective behaviour theory, the springtail system may offer a tractable model for studying proximity-mediated mechanical coupling in the absence of cognitive social interaction, making them an ideal empirical system for testing theoretical predictions about cascade propagation in random spatial networks.

Summary

This study provides a quantitative investigation of density-dependent collective escape response dynamics in springtails, combining high-quality slow-motion video recording with individual level manual tracking and a multi metric computational analysis pipeline. Six petri dish arenas, three low and three high densities, were analysed across different collective behaviour metrics and a multivariate PCA over the first second of the escape response after a standardised mechanical disturbance.

The central finding is that population density acts as a coupling parameter for the collective escape cascade. High-density plates showed approximately four times greater pairwise speed synchrony than low-density plates (mean Spearman r = 0.143 vs. 0.037), a stronger initial centrifugal escape burst, and smaller centre-of-mass displacement, consistent with proximity-mediated mechanical triggering operating over a denser and therefore more highly connected interaction network. At the same time, neither density condition produced meaningful directional alignment at any point during the recording: group polarisation remained below $\Phi = 0.13$ across all plates and conditions. The spatial–behavioural correlation analysis provided additional evidence for a density-dependent shift in interaction topology, from distance-limited local coupling in sparse groups to effectively all-to-all coupling in the densest plate (P5T3, n = 470), where spatial proximity no longer predicted behavioural similarity.

The multivariate PCA confirmed that the collective behaviour phenotype of high-density plates is distinguishable from that of low-density plates along a primary axis dominated by speed synchrony and escape geometry (PC1: 59.3% variance), though the separation was imperfect: P1T3 (Low) and P2T3 (High) both occupied intermediate positions in PC space, underlining that density does not deterministically fix the collective response profile of any individual plate.

Several important methodological limitations must be acknowledged. The sample size of three plates per density group was insufficient for statistical significance in any metric. The manual disturbance protocol introduced uncontrolled variability in stimulus delivery that an automated mechanism would eliminate. These constraints mean that all quantitative findings should be interpreted as preliminary trends requiring replication.

The primary contribution of this thesis is therefore methodological and conceptual rather than conclusive. The complete analytical pipeline, from raw CVAT annotation through individual tracking, collective metric computation, spatial grid analysis, and multivariate PCA, is fully documented and immediately applicable to any new dataset of springtail recordings.

The logical flow of the analysis, from individual-level kinematics through to population-level coupling metrics, provides a validated template for future studies of any collective escape behaviour in invertebrates. Additionally, extending the recording window from one second to five to ten seconds would allow characterisation of the full temporal profile of the escape cascade, including recovery dynamics that may also show density-dependent structure.

In summary, this study indicates that springtail population density systematically modulates the temporal synchrony and spatial geometry of collective escape responses through a proximity-based mechanical cascade mechanism, without generating the directional coordination characteristic of classical flocking. The analytical framework established here provides both the tools and the conceptual foundation for the more definitively powered studies that will be needed to fully characterise this system.

References

Ariel, G. and Ayali, A. (2015) 'Locust collective motion and its modeling', *PLOS Computational Biology*, 11(12), e1004522. https://doi.org/10.1371/journal.pcbi.1004522

Bode, N.W.F., Wood, A.J. and Franks, D.W. (2011) 'The impact of social networks on animal collective motion', *Animal Behaviour*, 82(1), pp. 29–38. https://doi.org/10.1016/j.anbehav.2011.04.011

Buhl, C., Sumpter, D. J., Couzin, I. D., Hale, J. J., Despland, E., Miller, E. R., & Simpson, S. J. (2006). From disorder to order in marching locusts. *Science*, *312*(5778), 1402-1406. https://doi.org/10.1126/science.1125142

Couzin, I.D., Krause, J., James, R., Ruxton, G.D. and Franks, N.R. (2002) 'Collective memory and spatial sorting in animal groups', *Journal of Theoretical Biology*, 218(1), pp. 1–11. https://doi.org/10.1006/jtbi.2002.3065

Couzin, I. D. (2009). Collective cognition in animal groups. *Trends in cognitive sciences*, 13(1), 36-43. https://doi.org/10.1016/j.tics.2008.10.002

De Winter, J. C., Gosling, S. D., & Potter, J. (2016). Comparing the Pearson and Spearman correlation coefficients across distributions and sample sizes: A tutorial using simulations and empirical data. *Psychological methods*, 21(3), 273. http://dx.doi.org/10.1037/met0000079

Domenici, P., Booth, D., Blagburn, J.M. and Bacon, J.P. (2011) 'Cockroaches keep predators guessing by using preferred escape trajectories', *Current Biology*, 21(18), pp. 1607–1610. https://doi.org/10.1016/j.cub.2011.08.006

Hopkin, S.P. (1997) Biology of the Springtails (Insecta: Collembola). Oxford: Oxford University Press.

Musleh, A., AlRyalat, S. A., & Qasem, A. (2023). Image Annotation Software for Artificial Intelligence Applications. *High Yield Medical Reviews*, 1(2). https://doi.org/10.59707/hymrXHMX8234

Nagy, M., Ákos, Z., Biro, D. and Vicsek, T. (2010) 'Hierarchical group dynamics in pigeon flocks', *Nature*, 464(7290), pp. 890–893. https://doi.org/10.1038/nature08891

Ozogány, K., Kerekes, V., Fülöp, A., Barta, Z. and Nagy, M. (2023) 'Fine-scale collective movements reveal present, past and future dynamics of a multilevel society in Przewalski's horses', *Nature Communications*, 14, 5096. https://doi.org/10.1038/s41467-023-40523-3

Romanczuk, P., Couzin, I.D. and Schimansky-Geier, L. (2009) ‘Collective motion due to individual escape and pursuit response’, *Physical Review Letters*, 102(1), 010602. https://doi.org/10.1103/PhysRevLett.102.010602

Sudo. S., Kainuma, T., Yano, T., Shirai, A., & Hayase, T. (2015). Jumps of water springtail and morphology of the jumping organ. *Journal of the Japanese Society for Experimental Mechanics*, 15 (Special_Issue), s117-s124.

Vicsek, T. and Zafeiris, A. (2012) ‘Collective motion’, Physics Reports, 517(3–4), pp. 71–140. https://doi.org/10.1016/j.physrep.2012.03.004